Wang, R. et al. (2013). Effect of the structure of Ni nanoparticles on the electrocatalytic activity of Ni@Pd/C for formic acid oxidation.
International Journal of Hydrogen Energy, 38(29): 13125 – 13131
http://dx.doi.org/10.1016/j.ijhydene.2013.01.104

Effect of the structure of Ni nanoparticles on the electrocatalytic activity of Ni@Pd/C for formic acid oxidation

Rongfang Wang, Hui Wang, Xingli Wang, Shijun Liao, Vladimir Linkov and Shan Ji

Abstract

Ni@Pd/C catalysts were synthesized, using Ni/C with different crystalline structures prepared with various ligands. A series of characterizations were performed by transmission electron microscopy, X-ray diffraction, X-ray photoelectron spectroscopy. The results indicated the electrocatalysts with amorphous/crystalline (denoted as Ni_a and Ni_c) Ni structures decorated with Pd. The formic acid electrocatalytic oxidation results showed that the peak current of Ni_a@Pd/C was about 1.2 times higher than that of Ni_c@Pd/C. The good electrochemical performance and stability of Pd-modified amorphous Ni substrate reveals that the core structure plays an important role in the electrocatalytic activity and the change of the structure can improve the activity and stability of electrocatalysts.

1. Introduction

If the goals of attaining practical power levels and reducing manufacturing costs are reached, direct formic acid fuel cells (DFAFC) may become promising alternative portable power sources [1e3]. Among problems that still need to be overcome are insufficient electro-catalytic activity of the anode catalyst for formic acid oxidation and catalyst deactivation due to formic acid oxidation on noble-metal catalysts that generates intermediates such as CO that can be adsorbed on the noble-metal catalysts' surface [4]. Although Pd/C electrocatalyst exhibited much better activity than Pt/C, its activity was still not satisfactory, and more importantly its durability was in urgent need for further improvement because of rapid deactivation of this catalyst [4e6]. Hence, it is important to develop new catalysts with high activity and stability for formic acid oxidation.

To increase the catalysis activity and reduce noble-metal loading, bimetallic catalysts of palladium alloyed with a non-noble-metal are often used [5,7e9]. Among different bimetallic catalysts, PdNi alloy catalyst has attracted most attention owing to its strong formic acid oxidation enhancement [10e12]. PdNi bimetallic alloy not only increases the active surface area of the Pd-based catalysts, offering more active sites necessary for the formic acid dissociation, but also results in the modification of electronic structure of palladium by Ni atoms which facilitate the removal of

poisoning intermediates on Pd [13]. However, PdNi alloy catalytic activity still remains a major limiting factor in the overall cell performance.

Recently, the tailored design of noble-metal bimetallic hetero-nanostructures has attracted considerable interest [14e17]. The catalytic properties of the hetero-nanostructures are strongly dependent on their sizes, shapes, and compositions [18]. A good control of the structural features and compositions is highly favorable for the creation of new noble metal nanocatalysts with enhanced catalytic performance and improved noble metal utilization efficiency [19]. Arranging noble metals as shells on proper non-noble metal cores not only greatly reduces their usage but also could significantly enhance their catalytic properties, as a result of the synergistic structural and electronic effects of the two metals [20]. In other words, the design of novel core and/or shell structure is a rational way to reduce the cost of the catalyst and enhance its activity and stability.

Compared to conventional crystalline metals, a metal in an amorphous state could present unique compositions and surface structures for molecular reactions, which make it interesting candidate for catalytic applications [21e23]. The lattice defects in an amorphous metal can result in not only distinct effects in mediating the electronic structure but also tuning the atomic arrangement and coordination of the outer shell of the catalyst [24e27]. Amorphous alloys have attracted much attention due to their superior electronic, magnetic, and chemical properties, as well as practical or potential applications in various fields [22,24,28].

On the basis of this concept, localization of Pd as a shell on an amorphous Ni core could be expected to both decrease the usage of Pd and enhance its catalytic activity. Although many studies have been focused on coreeshell structured nanoparticles, employing amorphous metal as a core has been rarely reported [26,29]. Thus, the synthesis of Ni@Pd coreeshell structure catalysts with Ni cores in different crystalline states and comparison of their catalytic activities is of great interest. In this article, a two-step method to prepare carbon supported palladium decorated nickel nanoparticles with different structures suitable for electrocatalystic applications and its formic acid oxidation activity and stability in a three-compartment electrochemical cell is presented.

2. Experimental

2.1 Preparation of Ni@Pd/C catalysts

In a typical procedure, Ni/C catalysts with different crystallinity were prepared by using two different ligands as follows. Nickel (II) chloride hexahydrate ($NiCl_2\$6H_2O$) (303 mg) was dissolved in solution containing 25 mL water and 25 mL ethanol. The ligands were added to the solution to produce different metal structures. To obtain crystal metal Ni (denoted as Ni_c/C), 750 mg sodium citrate was used; and for amorphous Ni (denoted as Ni_a/C), 760 mg EDTA was used. The pH of

the system was adjusted to w14 by the addition of KOH with vigorous stirring for 0.5 h. Pretreated carbon black Vulcan XC72R (300 mg) was added to the mixture under stirring. Subsequently, 15 mL of hydrazine hydrate was added. The mixture was then transferred to a Teflon lined autoclave and the temperature was maintained at 120 ^{0}C for 4 h. The resultant precipitate was collected by filtration, washed 5 times with deionized water and dried in vacuum at 60 ^{0}C for 12 h.

Afterward, 41.7 mg of $PdCl_2$ was transferred into two 100 mL beakers. Two drops of concentrated HCl acid was added to each beaker, and then the mixture was treated in an ultrasonic bath for several minutes. After that, 30 mL of ethylene glycol (EG) were introduced into the $PdCl_2$ mixture. Its pH value was adjusted to w10 by 5% KOH/EG solution. The Ni_a/ C and Ni_c/C powders obtained earlier were added to the each flask and the mixture was sonicated for 30 min. Subsequently, the mixture was heated at 160 ^{0}C for 8 h. The product was collected by filtration, rinsed 10 times with deionized water and dried overnight in a vacuum oven. The products were denoted Ni_a@Pd/C and Ni_c@Pd/C.

2.2. Characterization

The catalysts were characterized by recording their X-ray diffraction (XRD) patterns on a Shimadzu XD-3A diffractometer, using filtered Cu-Ka radiation. Transmission electron microscopy (TEM) measurements were carried out on a JEM-2010 electron microscope with the acceleration voltage of 200 kV. X-ray photoelectron spectroscopy (XPS) (PHI-5702 America) was conducted with a monochromatic Al Ka X-ray source (hn ¼ 29.35 eV). The chemical composition of the samples was determined using the energy dispersive X-ray analysis (EDX) technique coupled to the TEM and an IRIS advantage inductively coupled plasma atomic emission spectroscopy (ICP-AES) system (Thermo, America).

The electrochemical measurements of catalysts were performed on an Autolab electrochemical work station PGSTAT128N. A common three-electrode electrochemical cell was used for the measurements. The counter and reference electrodes were a platinum wire and an Ag/AgCl (3 M KCl) electrode, respectively. The working electrode was a glassy carbon disk (5 mm in diameter). The thin-film electrode was prepared as follows: 5 mg of catalyst was dispersed ultrasonically in 1 mL Nafion/ethanol (0.25% Nafion). 8 mL of the dispersion was transferred onto the glassy carbon disk using a pipette, and then dried in the air. The catalysts were characterized by cyclic voltammetry (CV) and chronoamperometry (CA) tests at room temperature. Before each measurement, the solution was purged with high purity N_2 gas for at least 30 min to ensure O_2 free measurements. All current density values in this article are normalized to the electrode surface area.

3. Results and discussion

Fig. 1 shows the XRD patterns of Ni_a@Pd/C, Ni_c@Pd/C, Ni_a/C and Ni_c/C nanoparticles. For comparison, the pattern of the carbon-supported Pd catalyst is also shown in this figure.

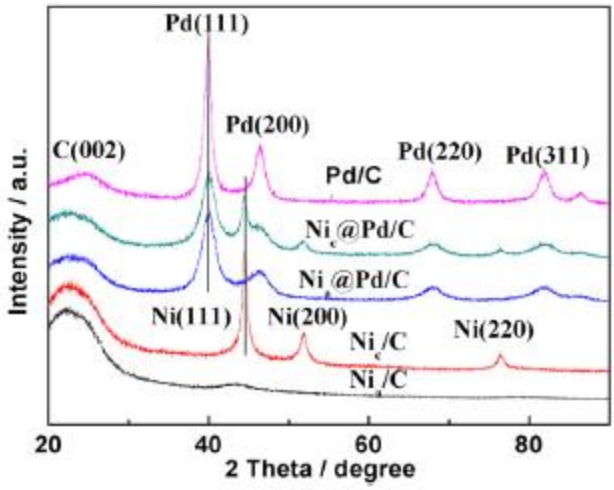

Fig. 1 – XRD patterns of Pd/C, Ni_a/C, Ni_c/C, Ni_a@Pd/C and Ni_c@Pd/C samples.

The first peak located at about 24.8º in all the XRD patterns is associated with the carbon support. For Ni_a/C, the slight broader peak at 2q values of ca. 42ºe48º suggests that the Ni is present in an amorphous structure. For the Ni_c/C, all of the peaks match well with Bragg reflections of the standard crystalline phase fcc structure. In accordance with ICDD file no: 04-0850, space group: Fm3m (225), the three peaks at ca. 44º, 52º and 76º can be assigned to their characteristic (111), (200) and (220) indices. The lattice parameter of the Ni_c/C nanoparticles was found to be ca. 0.35 nm. This is in agreement with the lattice parameter for bulk Ni metal. Compared with Ni_c/C, Ni_a/C in an amorphous state holds many more lattice defects and thus could produce distinct effects in mediating the electronic structure and/or tuning the atomic arrangement and coordination of the outer shell of the catalyst. For the Pd/C catalyst, the five peaks located at 2q values of ca. 40º, 47º , 68º , 83º , and 86º corresponded to the characteristic (111), (200), (220), (311), and (222) planes of fcc Pd crystal, respectively.

After depositing Pd on Ni nanoparticles via a reduction reaction, both of Ni_a@Pd/C and Ni_c@Pd/C catalysts exhibited the diffraction peaks around 40º, 47º , 68º , 83º , and 86º, which agree with Pd/C structure assigned to the Pd-shell. For the Ni_c@Pd/C catalysts, well separated diffraction peaks strongly suggest the presence of different phases. Diffraction peaks at 44.5º, 51.8º and 76.3º are in agreement with a metallic Ni structure assigned to the Ni-core. For the Ni_a@Pd/C

catalyst, no diffraction peaks were detected for Ni phase. The diffraction angle phases of the shell and the core for Ni_c@Pd/C and Ni_a@Pd/C samples are not shifted to higher or lower angles than those for Pd/C and Ni/C, indicating that no alloy phase was formed.

Fig. 2 shows TEM, high resolution TEM (HRTEM) and EDX pattern of Ni_a@Pd/C and Ni_c@Pd/C catalysts. It can be noted that the Ni_a@Pd/C and Ni_c@Pd/C nanoparticles are highly dispersed on the carbon support with the narrow size distribution. The uniform particle dispersion of Ni_a@Pd/C and Ni_c@Pd/C catalysts may result from the homogeneous size distribution of Ni core nanoparticles on carbon support. The Pd nanoparticles grow on Ni substrate rather than carbon support mainly because the interactions between metals and defective carbon are weaker than those between metals and metals. The TEM image shows that the size of Ni_a@Pd/C particles is smaller than that of Ni_c@Pd/C. The average particle size of Ni_a@Pd/C and Ni_c@Pd/C catalyst is approximately 4.8 nm and 5.2 nm, respectively, which is obtained from the measurement which involved one hundred particles. The selected area electron diffraction (SAED) pattern (inset of Fig. 2D) of Ni_c@Pd/C catalyst showed concentric rings, composed of bright discrete diffraction spots, that were indexed to (111), (220), (311), and (331) crystal planes of fcc structure, indicating the high degree of crystallinity of individual nanoparticles. However, the SAED pattern (inset in Fig. 2A) of Ni_a@Pd/C only shows inexplicit rings, thus indicating that the core of Ni_c@Pd/C catalysts exists mainly in the amorphous state.

A HRTEM study of a series of Ni_a@Pd/C (Fig. 2B) and Ni_c@Pd/ C (Fig. 2E) catalysts shows that Pd on the surface of the nanoparticles has a polycrystalline structure. The measured distance between the two nearest atom rows for Ni_a@Pd/C and Ni_c@Pd/C is 0.22 nm, which is close to the (111) interplanar distance of pure Pd, suggesting that Pd atoms are dispersed on the outer layer of Ni particles and not alloyed with Ni nanoparticles. The EDX result indicates the atomic ratio of Pd/Ni of Ni_a@Pd/C and Ni_c@Pd/C is ca. 1:1.2 and 1:1.9, respectively (as shown in Fig. 2C and F).

X-ray photoelectron spectroscopy (XPS) was used to determine the surface composition and the surface oxidation states of the catalytic metals. The spectrum corresponding to Pd 3d indicates the presence of Pd in two different oxidation states (0 and II) with the predominance of the metallic state. As displayed in Fig. 3, the spectrum showed only two asymmetric Pd peaks assigned to Pd $3d_{5/2}$ and Pd $3d_{3/2}$ having a binding energy of 341 eV and 336 eV, typical of Pd metal. The peaks of Pd $3d_{5/2}$ at around 342 eV and Pd $3d_{3/2}$ at 337 eV are assigned to Pd(II) in PdO [30]. Comparison of binding energies of Pd $3d_{5/2}$ and Pd $3d_{3/2}$ for Ni_c@Pd/C and Ni_a@Pd/C is presented in Table 1.

The percentages of Pd (0) and Pd (II) for Ni_c@Pd/C and Ni_a@Pd/C were obtained by calculating the relative areas of corresponding peaks, which are 95.3% of Pd (0) and 4.7% of Pd (II) in Ni_c@Pd/C; 71.1% of Pd (0) and 28.9% of Pd(II) in Ni_a@Pd/C. The results show that the amount of Pd in metallic state in Ni_c@Pd/C is more than that in Ni_a@Pd/C. Pd (0) plays a principal role in Ni_a@Pd/C catalyst, which is consistent with the XRD pattern result. It is noticed that there are slight shifts in binding energies of the Pd $3d_{5/2}$ and $3d_{3/2}$ between Ni_c@Pd/C and Ni_a@Pd/C, which may be caused by atom rebuilt of Pd and Ni resulting in charge transfer occurring between Pd and Ni phases. The positive shift of the Pd $3d_{5/2}$ and $3d_{3/2}$ binding energies in Ni_a@Pd/C can be attributed to the interaction between pure Pd and the adjacent Ni, accompanied by rehybridization of the d-band as well as the sp-band.

Typical voltammograms of Ni_a@Pd/C and Ni_c@Pd/C catalysts in 0.5 mol L^{-1} H_2SO_4 solution are shown in Fig. 4a. The adsorption/desorption peak of atomic hydrogen on the nanostructure can be observed between -0.2 and 0.1 V vs. Ag/AgCl. The large anodic peak at more negative potential is related to hydrogen desorption from the bulk of particles, whereas the small anodic one at more positive potential is ascribed exclusively to oxidation of hydrogen adsorbed on the surface of particles.

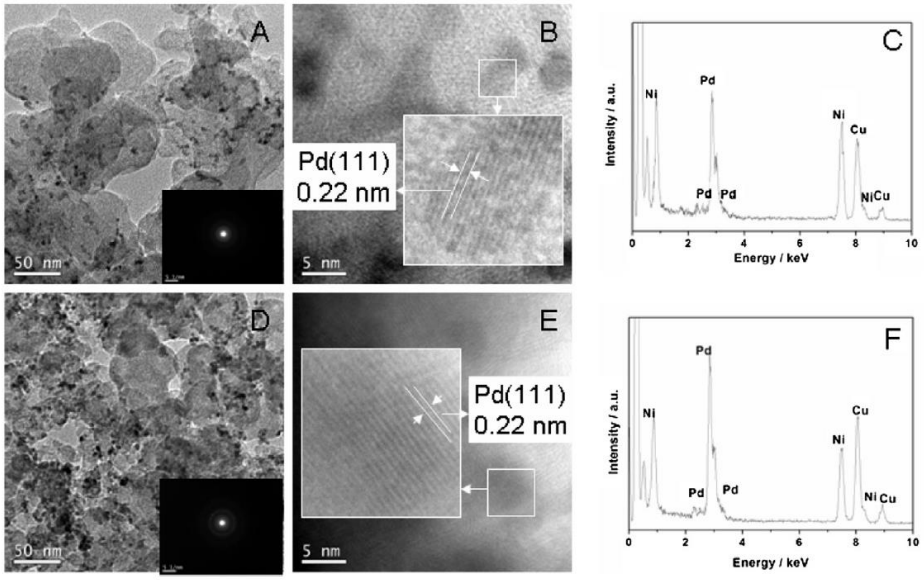

Fig. 2 – TEM, HRTEM and EDS images of Ni_a@Pd/C (A, B and C) and Ni_c@Pd/C (D, E and F) catalysts. Inset of (A) and (D) show the SAED patterns of Ni_a@Pd/C and Ni_c@Pd/C catalysts.

The formation of cathodic peak is considered to be an inverse process of hydrogen desorption, more exactly the adsorption of hydrogen on the particle surface. The

well-established features of hydrogen adsorption and desorption, double layer charging, oxide formation, and oxide reduction are evident in both samples, indicating that the surface of Ni_a@Pd/C and Ni_c@Pd/C catalysts are covered by Pd layer.

CO poisoning is a major issue for current application of noble metals as catalyst in fuel cells because the active- specific area (S_{EAS}) of the catalyst is reduced during operation due to adsorption of CO molecules that are generated from the partial oxidation of formic acid and diffuse through the membrane into the cathode. The CVs for CO electro-oxidation on the catalysts of Ni_a@Pd/C and Ni_c@Pd/C are shown in Fig. 4b. It can be observed that hydrogen desorption peaks for both catalysts are absent in the first scan in the hydrogen region of the CO stripping curve (-0.2 to 0.1 vs Ag/ AgCl), this indicating nearly complete coverage of Pd active sites with CO. However, hydrogen desorption peaks recover in the second cycle after CO is completely removed by oxidation. It can be seen that the onset potential of CO electro-oxidation with Ni_a@Pd/C (0.69 V) is lower than that of Ni_c@Pd/C (0.73 V), which demonstrates that crystallinity of Ni influences the CO oxidation ability (the onset oxidation potential). The peak potential of Ni_a@Pd/C and Ni_c@Pd/C are 0.82 V and 0.83 V, respectively. The lower peak potential and onset potential of CO_{ads} oxidation on Ni_a@Pd/C indicate that Ni_a@Pd/C catalyst is kinetically more active for this process [31]. The S_{EAS} of the catalyst is calculated using the equation [32]:

$$S_{EAS} = \frac{Q_{CO}}{484w} \qquad (1)$$

where S_{EAS} is the electrochemical active surface area of different catalysts, Q_{CO} is the charge for CO desorption electro-oxidation in microcoulombs (mC), 484 is the charge required to oxidize a monolayer of CO on the catalyst in mC cm^{-2} and w is the Pd loading, respectively. The results of S_{EAS} are 64.55 and 57.60 m^2 g^{-1}, for Ni_c@Pd/C and Nia@Pd/C, respectively.

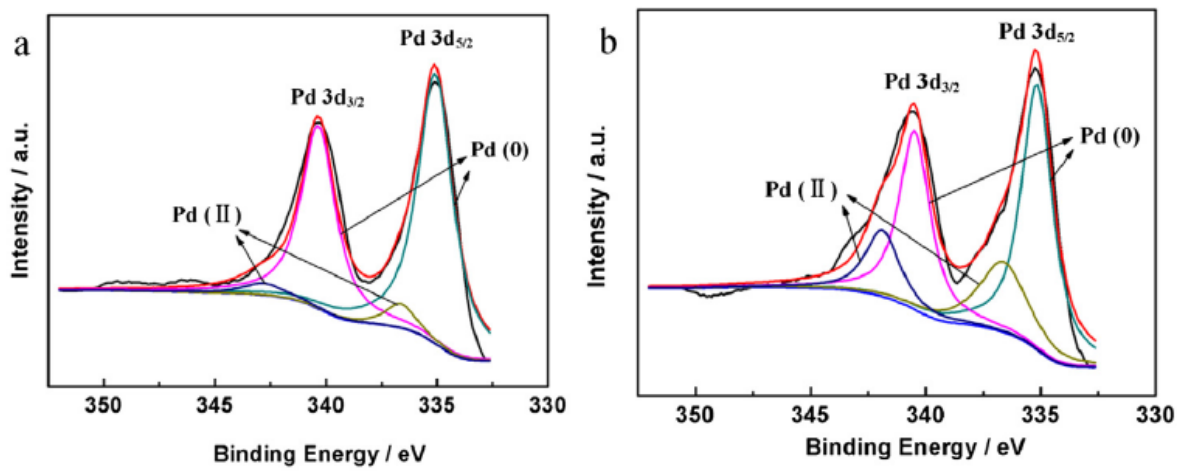

Fig. 3 – Pd 3d (a) XPS spectra of Pd@Ni$_c$/C catalysts; (b) XPS spectra of Pd@Ni$_a$/C catalysts.

Table 1 – Binding energies of Pd 3d$_{5/2}$ and Pd 3d$_{3/2}$ for Ni$_a$@Pd/C and Ni$_c$@Pd/C catalysts.

Electro orbit	Samples	Binding energies (eV)	
		Pd(0)	Pd(II)
Pd 3d$_{5/2}$	Ni$_a$@Pd/C	335.20	336.69
	Ni$_c$@Pd/C	335.08	336.64
Pd 3d$_{3/2}$	Ni$_a$@Pd/C	340.49	341.19
	Ni$_c$@Pd/C	340.38	342.79

Fig. 4c presents the CV results for the Ni$_a$@Pd/C and Ni$_c$@Pd/C samples in a 0.5 mol L^{-1} HCOOH þ 0.5 mol L^{-1} H_2SO_4 solution. The peak current of Ni$_a$@Pd/C and Ni$_c$@Pd/C catalysts are 15.25 mA cm^{-2} and 13.15 mA cm^{-2}, respectively. The higher HCOOH oxidation current suggests that Ni$_a$@Pd/C catalyst exhibits better HCOOH electro-oxidation activity than the catalyst Ni$_c$@Pd/C, mainly because of the modified electronic states and/or adjustment of atomic arrangement in Pd influenced by the amorphous metal Ni.

It has been reported that the electrooxidation of formic acid on Pd nanoparticles adopts a dual path mechanism, a dehydrogenation path to the direct formation of CO_2 and a dehydration path, and that the adsorption of CO intermediate from the dehydration path significantly poisons the activity of Pd catalysts [21] according to the following mechanism:

$$HCOOH \rightarrow CO_2 + 2H^+ + 2e^- \quad (2)$$

$$HCOOH \rightarrow CO_{ads} + H_2O \quad (3)$$

$$CO_{ads} + H_2O \rightarrow CO_2 + 2H^+ + 2e^- \quad (4)$$

The reaction of dehydration (2) as the main path is by many orders of magnitude more efficient than the paths 3 and 4. It is obvious that the current density of the peak at around 0.2 V (through the direct pathway) is much larger than that at 0.4e0.5 V representing the CO pathway. Thus it can be suggested that the oxidation of formic acid on both prepared catalysts proceeded mainly through the direct pathway.

Fig. 4d shows the chronoamperometric curves of formic acid oxidation in 0.5 mol L^{-1} HCOOH in 0.5 mol L^{-1} H_2SO_4 solution at 0.1 V vs. Ag/AgCl at room temperature on Ni_a@Pd/C and Ni_c@Pd/C electrodes. When the potential is fixed, continuous formic acid oxidation occurs on the electrocatalyst surface at 0.1 V vs. Ag/AgCl. A decrease of current density was recorded at the beginning of the experiment. Both Ni_a@Pd/C and Ni_c@Pd/C electrodes showed rapid current decay and low final current density. This indicates that the Ni_a@Pd/C and Ni_c@Pd/C surface is prone to poisoning by formic acid.

Long-term poisoning rates (ð) were obtained by measuring the liner decay of the current at times greater than 500 s using the following equation [33]:

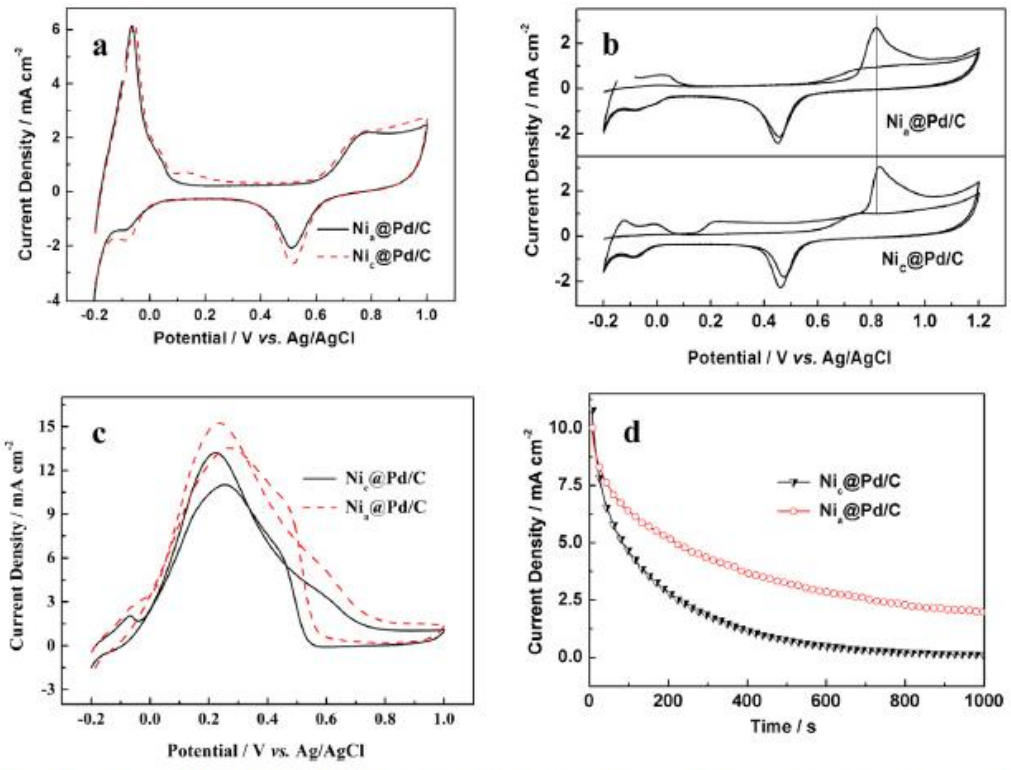

Fig. 4 – (a) CVs of Ni_a@Pd/C and Ni_c@Pd/C catalysts in 0.5 mol L^{-1} H_2SO_4 solution under N_2 atmosphere; scan rate: 50 mV s^{-1}; (b) CO stripping voltammograms of Ni_a@Pd/C and Ni_c@Pd/C catalysts in an N_2 saturated solution of 0.5 mol L^{-1} H_2SO_4; (c) CVs of Ni_a@Pd/C and Ni_c@Pd/C catalysts in 0.5 mol L^{-1} H_2SO_4 solution containing 0.5 mol L^{-1} formic acid under N_2 atmosphere; scan rate: 50 mV s^{-1}; (d) CAs of Ni_a@Pd/C and Ni_c@Pd/C in 0.5 mol L^{-1} HCOOH + 0.5 mol L^{-1} H_2SO_4 solution at 0.1 V vs Ag/AgCl.

$$\delta = \frac{100}{i_0} \times \left(\frac{di}{dt}\right)_{t>500} \quad (5)$$

where ðdi=dtÞ t>500 is the slope of the linear portion of the current decay and i0 is the current at the start of polarization back-extrapolated from the linear current decay, respectively. It is established that the formic acid oxidation reaction proceeds through the formation of reactive intermediates (HCOOads) and the ultimate poisoning species (COads) on the Pd group of metals. The d of Nia@Pd/C and Nic@Pd/C is 0.08 and 0.10, indicating that Nia@Pd/C is more stable catalyst.

4. Conclusions

Carbon-supported Ni@Pd coreeshell nanoparticulate catalysts with different crystallization degree of Ni are synthesized and characterized. The results of XRD, TEM and XPS showed that amorphous/crystalline Ni as a seed impacts on the structure of Pd outer layer. Electrochemical results proved that Pd reduced on amorphous Ni substrate has better electrochemical performance, which was attributed to the unique structure of amorphous metal. Thus, controlling the crystallinity of Ni substrate by using different ligands represents a promising approach to improve the catalytic activity of coreeshell Ni@Pd bimetallic catalyst nanoparticles toward formic acid oxidation.

Acknowledgments

We greatly appreciate the National Natural Science Foundation of China (21163018), the National Science Foundation for Post-doctoral Scientists of China (20110490847, 2012T50554), the research fund of the Key Laboratory of Fuel Cell Technology of Guangdong Province and the South African NRF (SFP20110918000027143) for financially supporting this work.

References

[1] Zhang S, Shao Y, Yin G, Lin Y. Electrostatic self-assembly of a Pt-around-Au nanocomposite with high activity towards formic acid oxidation. Angew Chem Int Ed 2010;49:2211e4.
[2] Rice C, Ha S, Masel RI, Waszczuk P, Wieckowski A, Barnard T. Direct formic acid fuel cells. J Power Sources 2002;111:83e9.
[3] Wang R, Liao S, Ji S. High performance Pd-based catalysts for oxidation of formic acid. J Power Sources 2008;180:205e8.
[4] Rice C, Ha S, Masel RI, Wieckowski A. Catalysts for direct formic acid fuel cells. J Power Sources 2003;115:229e35.
[5] Zhu Y, Khan Z, Masel RI. The behavior of palladium catalysts in direct formic acid fuel cells. J Power Sources 2005;139: 15e20.
[6] Lee H, Habas SE, Somorjai GA, Yang P. Localized Pd overgrowth on cubic Pt nanocrystals for enhanced electrocatalytic oxidation of formic acid. J Am Chem Soc 2008;130:5406e7.
[7] Liu ZL, Zhang XH, Tay SW. Nanostructured PdRu/C catalysts for formic acid oxidation. J Solid State Electrochem 2012;16: 545e50.
[8] Lu Y, Chen W. Nanoneedle-covered Pd-Ag nanotubes: high electrocatalytic activity for formic acid oxidation. J Phys Chem C 2010;114:21190e200.
[9] Zhou W, Lee JY. Highly active coreeshell Au@Pd catalyst for formic acid electrooxidation. Electrochem Commun 2007;9: 1725e9.
[10] Leonard BM, Zhou Q, Wu D, DiSalvo FJ. Facile synthesis of PtNi intermetallic nanoparticles: influence of reducing agent and precursors on electrocatalytic activity. Chem Mater 2011; 23:1136e46.
[11] Du C, Chen M, Wang W, Yin G, Shi P. Electrodeposited PdNi2 alloy with novelly enhanced catalytic activity for electrooxidation of formic acid. Electrochem Commun 2010; 12:843e6.
[12] Du C, Chen M, Wang W, Yin G. Nanoporous PdNi alloy nanowires as highly active catalysts for the electro-oxidation of formic acid. ACS Appl Mater Interfaces 2010;3:105e9.
[13] Chen L, Guo H, Fujita T, Hirata A, Zhang W, Inoue A, et al. Nanoporous PdNi bimetallic catalyst with enhanced electrocatalytic performances for electro-oxidation and oxygen reduction reactions. Adv Funct Mater 2011;21:4364e70.
[14] Wang L, Yamauchi Y. Strategic synthesis of trimetallic Au@Pd@Pt Core-Shell nanoparticles from poly(vinylpyrrolidone)-based aqueous solution toward highly active electrocatalysts. Chem Mater 2011;23:2457e65.
[15] Xing Y, Cai Y, Vukmirovic MB, Zhou W-P, Karan H, Wang JX, et al. Enhancing oxygen reduction reaction activity via
Pd-Au alloy sublayer mediation of Pt monolayer electrocatalysts. J Phys Chem Lett 2010;1:3238e42.
[16] Yancey DF, Carino EV, Crooks RM. Electrochemical synthesis and electrocatalytic properties of Au@Pt dendrimer-encapsulated nanoparticles. J Am Chem Soc 2010;132:10988e9.

[17] Wang XL, Wang H, Wang RF, Wang QZ, Lei ZQ. Carbon-supported platinum-decorated nickel nanoparticles for enhanced methanol oxidation in acid media. J Solid State Electrochem 2012;16:1049e54.
[18] Bing Y, Liu H, Zhang L, Ghosh D, Zhang J. Nanostructured Pt-alloy electrocatalysts for PEM fuel cell oxygen reduction reaction. Chem Soc Rev 2010;39:2184e202.
[19] Qiao Y, Li CM. Nanostructured catalysts in fuel cells. J Mater Chem 2011;21:4027e36.
[20] Alayoglu S, Nilekar AU, Mavrikakis M, Eichhorn B. RuePt coreeshell nanoparticles for preferential oxidation of carbon monoxide in hydrogen. Nat Mater 2008;7:333e8.
[21] Barroso J, Pierna AR, Blanco TC, Moralló n E, Huerta F. Acetic acid decarboxylation by amorphous alloys with low loading of platinum. Int J Hydrogen Energy 2011;36:12574e82.
[22] Barranco J, Pierna AR. Amorphous $Ni_{59}Nb_{40}Pt_{(1-x)}Y_X$ modified carbon paste electrodes and their role in the electrochemical methanol deprotonation and CO oxidation process. J Non-Cryst Solids 2007;353:851e4.
[23] Jacobson LC, Molinero V. Can amorphous nuclei grow crystalline clathrates? The size and crystallinity of critical clathrate nuclei. J Am Chem Soc 2011;133:6458e63.
[24] Wen M, Liu H, Zhang F, Zhu Y, Liu D, Tian Y, et al. Amorphous FeNiPt nanoparticles with tunable length for electrocatalysis and electrochemical determination of thiols. Chem Commun 2009:4530e2.
[25] Sistiaga M, Pierna AR. Application of amorphous materials for fuel cells. J Non-Cryst Solids 2003;329:184e7.
[26] Zhang X-B, Yan J-M, Han S, Shioyama H, Xu Q. Magnetically recyclable Fe@Pt Core-Shell nanoparticles and their use as electrocatalysts for ammonia borane oxidation: the role of crystallinity of the core. J Am Chem Soc 2009;131:2778e9.
[27] Zhang XT, Wang H, Key JL, Linkov V, Ji S, Wang XL, et al. Strain effect of coreeshell Co@Pt/C nanoparticle catalyst with enhanced electrocatalytic activity for methanol oxidation. J Electrochem Soc 2012;159:B270e6.
[28] Asami K, Kawashima A, Hashimoto K. Chemical properties and applications of some amorphous alloys. Mater Sci Eng 1988;99:475e81.
[29] Wang H, Zhang X, Wang R, Ji S, Wang W, Wang Q, et al. Amorphous CoSn alloys decorated by Pt as high efficiency electrocatalysts for ethanol oxidation. J Power Sources 2011; 196:8000e3.
[30] Meng H, Xie F, Chen J, Shen PK. Electrodeposited palladium nanostructure as novel anode for direct formic acid fuel cell. J Mater Chem 2011;21:11352e8.
[31] Cui Z, Kulesza PJ, Li CM, Xing W, Jiang SP. Pd nanoparticles supported on HPMo-PDDA-MWCNT and their activity for formic acid oxidation reaction of fuel cells. Int J Hydrogen Energy 2011;36:8508e17.
[32] Zhou C, Wang H, Peng F, Liang J, Yu H, Yang J. MnO_2/CNT supported Pt and PtRu nanocatalysts for direct methanol fuel cells. Langmuir 2009;25:7711e7.

[33] Jiang J, Kucernak A. Electrooxidation of small organic molecules on mesoporous precious metal catalysts I: CO and methanol on platinum. J Electroanal Chem 2002;533:153e65.